OPEN ACCESS
IOP Publishing
Plasma Physics and Controlled Fusion
Plasma Phys. Control. Fusion **57** (2015) 045008 (8pp)
doi:10.1088/0741-3335/57/4/045008

High-Speed imaging of the plasma response to resonant magnetic perturbations in HBT-EP

Sarah M Angelini, Jeffrey P Levesque, Michael E Mauel and Gerald A Navratil

Columbia University, New York, NY 10027, USA

E-mail: angelini@caa.columbia.edu, jpl2131@columbia.edu, mauel@columbia.edu and gan2@columbia.edu

Received 4 November 2014, revised 12 January 2015
Accepted for publication 29 January 2015
Published 12 March 2015



Abstract

A Phantom v7.3 fast digital camera was used to study visible light fluctuations in the High Beta Tokamak–Extended Pulse (HBT–EP). This video data is the first to be used to analyze and understand the behavior of long wavelength kink perturbations in a wall-stabilized tokamak. The light was mostly comprised of Dα 656 nm light. Profiles of the plasma light at the midplane were hollow with a radial scale length of approximately 4 cm at the plasma edge. The fast camera was also used to measure the plasma's response to applied helical magnetic perturbations. The programmed toroidal phase angle of the resonant magnetic perturbation (RMP) was directly inferred from the resulting images of the plasma response. The plasma response and the intensity of the RMP were compared under different conditions. The resulting amplitude correlations are consistent with previous measurements of the static response using an array of magnetic sensors.

Keywords: tokamaks, MHD instabilities, high-speed videography, magnetic perturbations

S Online supplementary data available from stacks.iop.org/PPCF/57/045008

(Some figures may appear in colour only in the online journal)

1. Introduction

Cameras and other visual diagnostics have become crucial for understanding a plasma's behavior in magnetic fusion research devices. These diagnostics can include photomultiplier tubes [1], photodiodes [2], and cameras. High-speed digital cameras, also known as fast cameras, have been used previously on tokamaks to study soft x-rays [3], and in the visible spectrum have captured edge localized modes (ELMs) [4–7], neoclassical tearing modes (NTMs) [8], dust [9], modes in the divertor region [10], and local behavior with gas puff imaging (GPI) [11]. Recently, light emission measurements have been shown to be useful in detecting the quasi-stationary MARFE-like structures as well as the helical modulation of small scale turbulence in a reverse field pinch [12]. In a stellarator, gated visible tomography has been used to detect the internal structure of rapidly rotating modes [13, 14].

This paper presents measurements from a high-speed video camera diagnostic on the High Beta Tokamak–Extended Pulse (HBT–EP) [15–17]. These measurements extend previous research on plasma videography and establish quantitative correlations between the amplitude and phase of visible light fluctuations, and those of edge magnetic field fluctuations. HBT–EP is a circular cross-sectioned large aspect ratio tokamak with dimensions $R = 0.92$ m, $a = 0.15$ m and a magnetic field of 0.35 T. HBT–EP is unique in that it has twenty internal movable wall segments ('shells') that permit different wall configurations. The simple presence of these shells can passively stabilize plasma perturbations, and moving them into different positions has a strong impact on the plasma's stability [18, 19]. In addition, 216 magnetic sensors give us a full view of the plasma's edge and aid in building a picture of



Content from this work may be used under the terms of the Creative Commons Attribution 3.0 licence. Any further distribution of this work must maintain attribution to the author(s) and the title of the work, journal citation and DOI.

 © 2015 IOP Publishing Ltd Printed in the UK

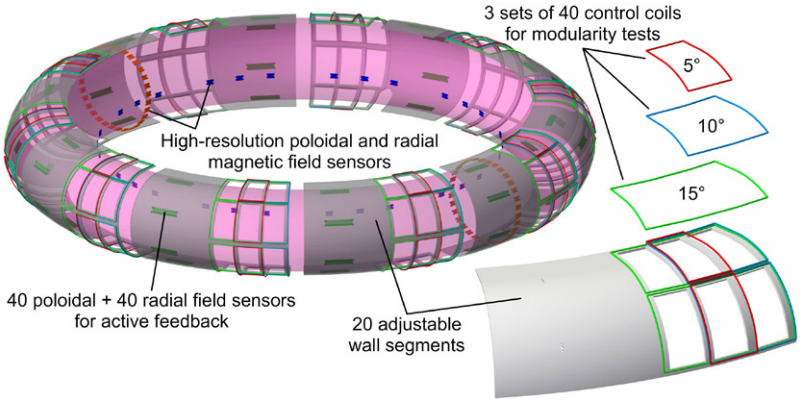


Figure 1. A diagram of the shells and sensors on HBT–EP.

the plasma's response to magnetic perturbations [17]. Figure 1 shows where the shells and sensors are located on HBT–EP and also includes the control coils. HBT–EP has three sets of 40 control coils which can be programmed independently to excite different plasma modes. The most recent work on HBT–EP has involved active feedback [20, 21] to drive the control coils in real-time to compensate for changing magnetic perturbations.

2. Experimental setup

A Vision Research Phantom v7.3 camera [22] was installed to capture the plasma's global behavior using visible light emissions. Because the magnetic fields near the chamber are stronger than the camera's tolerance, a 48 inch Schott IG-163 imaging optical fiber cable [23] was used to carry the light from the zoom lens at the port to the first of two 50 mm lenses at the camera. The two 50 mm lenses allowed a filter to be placed between them. During some measurements, a Dα filter was used, but measurements by a spectrometer confirmed that the Dα light dominated. The light emission and the image structures were found to remain unchanged without the filter. This is consistent with the light expected from interactions between neutral deuterium and plasma electrons.

The camera was operated at frame rates from 63 to 125 kfps. Because the temporal resolution of the images decreases as the spatial resolution is increased, a balance between them was necessary to properly resolve the plasma movement. The ideal spatial resolution was determined to be 128 × 128 pixels at a frame rate of 88 kfps.

Inside the tokamak, the stainless steel vacuum vessel and the movable chrome-coated shells are reflective. To record light directly from the plasma and prevent reflections, a 140 mm by 775 mm sheet of aluminum, coated with Acktar Spectral Black™, was attached to the vessel wall with welded studs. The shells could be moved away from the black background for inversion measurements, or moved in front of the background to protect it from the plasma when the background wasn't needed. Figure 2 shows the camera view with the shells retracted, and in figure 3, viewing paths can be seen. The black material is revealed in the gap separating the wall segments.

Figure 3 also demonstrates the relationship between the camera's toroidal viewing angle and the representative

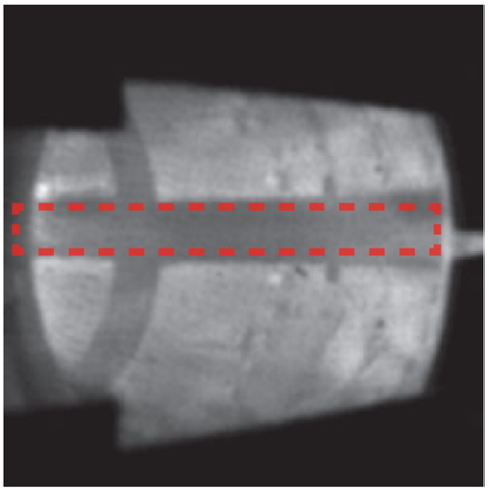


Figure 2. View of the plasma with the shells retracted. The black background spans the width in the center of the image as indicated by the dotted red rectangle.

magnetic diagnostics. Within the camera's view are shell segments with a poloidal array of 48 Mirnov detectors, described in [17]. These detectors allow for correlation measurements between the orientation of the magnetic perturbations and the structure of the visible light fluctuations.

3. Abel inversion results

The camera in combination with the black background can provide information about the radial profile of the light. First, a linear array of data was created from the 2D images. A rectangle of pixels corresponding to the light in front of the black background was extracted from each 2D image in the data video. This rectangle was then averaged in the vertical direction, creating a horizontal array of about 110 pixels. Because the black background was located at the midplane of the tokamak, the resulting array represents the line-integrated light emission across a series of tangential chords in the major radial direction. An Abel inversion is then applied using the method described by Álvarez *et al* [24] as shown in equation (1) where $I(x_i)$ is the line-integrated signal of each pixel i at radius x_i and $\epsilon(r_j)$ is the inverted signal at radius r_j:

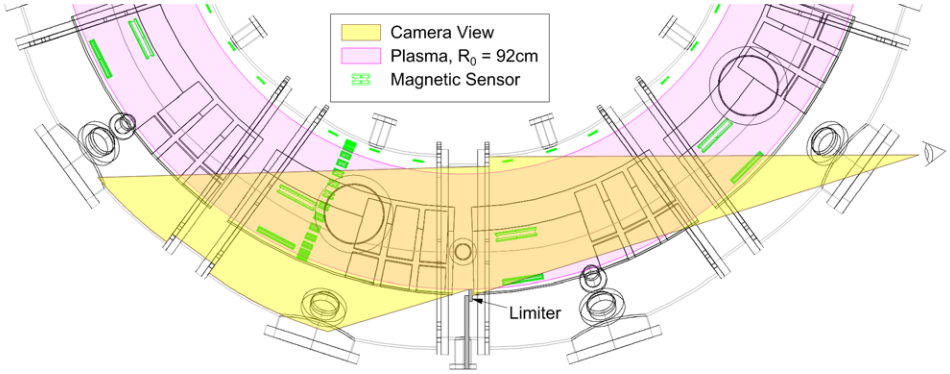


Figure 3. An overhead view of HBT–EP showing the viewing paths for the fast camera. The viewing angle is approximately 36 degrees. The locations of the magnetic sensors are also indicated. Because of the limited space for the lenses, a mirror was used. All the images recorded by the fast camera will appear mirror-reversed.

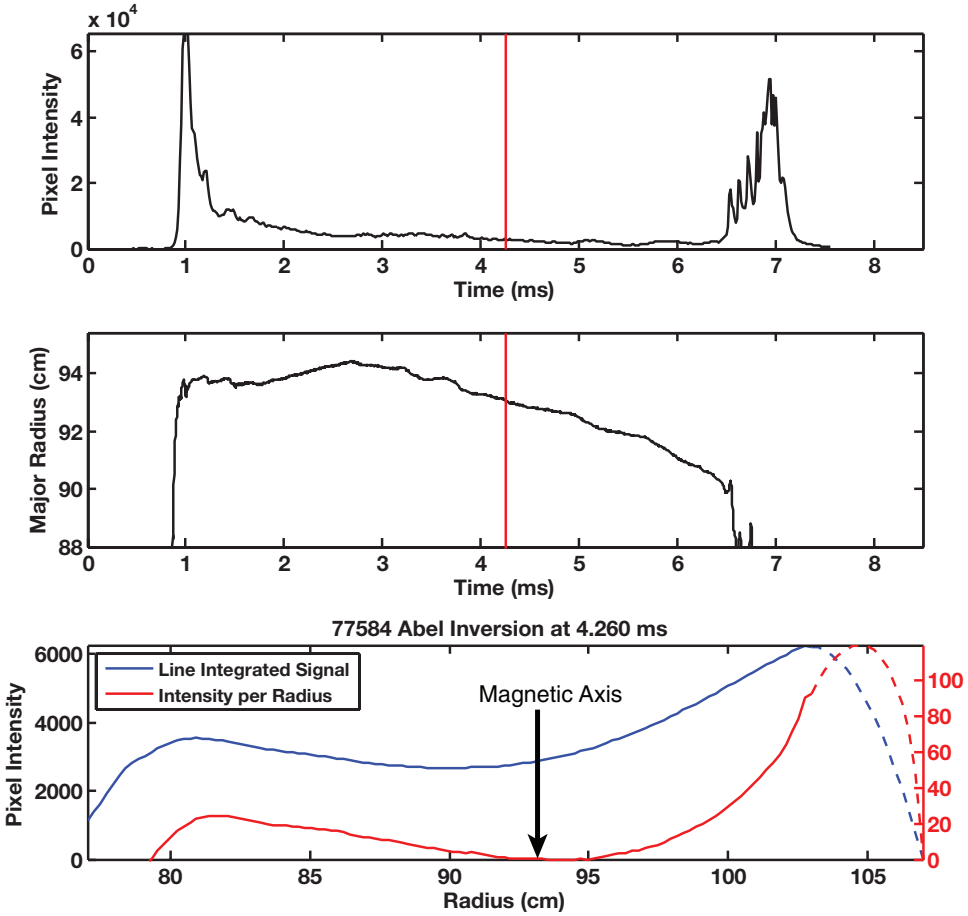


Figure 4. An Abel inversion for Shot 77584. The top plot is a single pixel trace in time, the second is the major radius of the plasma centroid, and the third displays the Abel inversion. 'Line Integrated Signal' in blue refers to the vertically-averaged data from the fast camera and 'Intensity per Radius' in red is the $\epsilon(r_j)$ inversion from equation (1).

$$\epsilon(r_j) = -\frac{1}{\pi}\sum_{i=j}^{N-1}\frac{I(x_{i+1}) - I(x_i)}{\sqrt{(x_i + \frac{\Delta x}{2})^2 - r_j^2}} \qquad (1)$$

Figure 4 shows the results of an Abel inversion for Shot 77584, an unforced plasma shot. The top graph is a plot of a single pixel over the course of the entire shot. It starts with a large increase in emissions around 1 ms which is a result of the breakdown and rapid ionization of injected neutral deuterium. After the formation of the plasma, the light decreases slightly in intensity throughout the shot until a disruption terminates the discharge at 6.5 ms. The middle graph shows the major radius of the plasma centroid through the shot and the lower graph shows, in blue, the linear signal created from averaging the pixels in the black rectangle at 4.26 ms as described above. The line-integrated signal (blue line) is dashed toward the right because the view of the very edge of the plasma is blocked by the outboard limiter. The light is assumed to drop

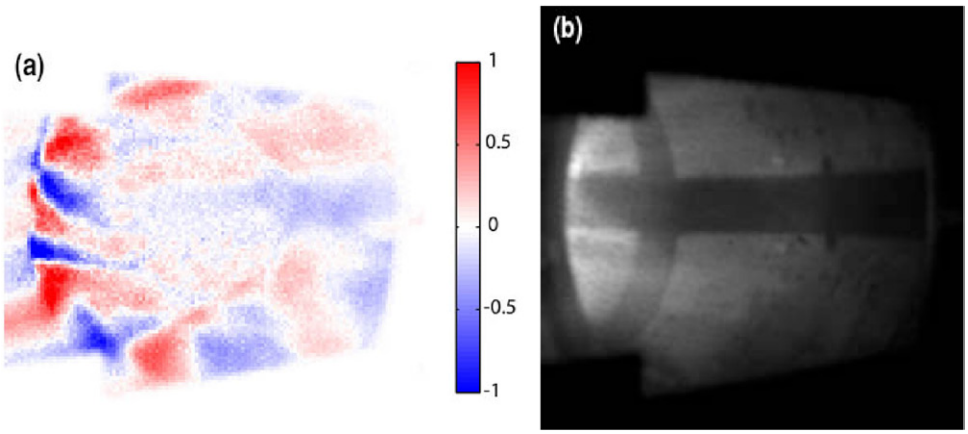


Figure 5. The result of the frame-by-frame subtraction (*a*) compared to the raw image (*b*) of Shot 76717 at time 4.174 ms. The red indicates increasing light, the blue is decreasing light, and the white shows no change in the light fluctuations.

off, so the edge is modelled using a quadratic polynomial. The computed local emission profile is shown in red and is the result of the inversion. The profile is hollow, which is to be expected because the central plasma is hot and dense enough to be nearly fully ionized. The light emission results from recycled neutrals at the edge [25].

4. Structure of the plasma fluctuations

While the Abel inversion was used to compute the static, non-perturbed intensity profile, it cannot easily provide any information about the plasma's fluctuations. One method for extracting these fluctuations is to perform an approximate background subtraction by taking each image and subtracting the one prior to it. The result is a series of images portraying the rate of change in light levels. At the standard frame rate of 88 000 fps, periodic oscillations can be detected without aliasing below 44 kHz, and images showing the change in intensity are computed, giving similar results to those using a high pass filter. Shot 76717 gives an example of where the difference subtraction is useful. The images were taken toward the end of the shot, within 100 μs of the disruption. Figure 5 shows the difference subtraction at time 4.174 ms when the edge safety factor was $q \sim 5$ and the mode oscillation frequency was relatively rapid, ~20 kHz. The difference image shows a many-lobed poloidal cross-section induced by helical perturbations that rotate in the electron drift direction. The image has been colored so that positive values, indicating an increase in the light level, are red, and negative values from decreasing light are blue.

The frame-by-frame subtraction works very well for fast-moving fluctuations, but for slow, steady plasmas, important signal information is not easily extracted. Instead of specifically designating aspects of the video as 'signal' and 'background' a different breakdown can be used to identify the dominant plasma behavior. A useful analysis method for this purpose is the biorthogonal decomposition (BD) [26, 27]. It is effectively a singular value decomposition (SVD) where the component matrices are the spatial and temporal modes that represent an orthogonal basis of the original 3D matrix of data.

The matrix of signals $\overrightarrow{S}$ is broken into a spatial matrix $\overrightarrow{V}$, a temporal matrix $\overrightarrow{U}$ and a diagonal matrix of singular values $\overrightarrow{\sigma}$ as shown in equation (2).

$$\begin{pmatrix} \uparrow & \uparrow & \\ \overrightarrow{s_1} & \overrightarrow{s_2} & \dots \\ \downarrow & \downarrow & \end{pmatrix} = \begin{pmatrix} \uparrow & \uparrow & \\ \overrightarrow{u_1} & \overrightarrow{u_2} & \dots \\ \downarrow & \downarrow & \end{pmatrix} \cdot \begin{pmatrix} \sigma_1 & & \\ & \sigma_2 & \\ & & \ddots \end{pmatrix} \cdot \begin{pmatrix} \leftarrow & \overrightarrow{v_1} & \rightarrow \\ \leftarrow & \overrightarrow{v_2} & \rightarrow \\ & \vdots & \end{pmatrix} \quad (2)$$

In the case of HBT–EP [17], the spatial modes show the geometry of the coherent structures and the temporal modes indicate how those structures move. Often the spatial structures appear to be rigidly rotating in the toroidal direction. The singular values give an indication of the strength of each mode. By recombining the dominant spatial and temporal modes, a picture of the plasma's coherent activity can be determined.

The biorthogonal decomposition has been used extensively on HBT–EP's magnetic probe signals [17, 28], but it can also be applied to the data from the fast camera. Figure 6 shows an example of the spatial and temporal BD modes for Shot 77324, a plasma without an applied magnetic perturbation, computed over 1.5 ms. The first 'mode' from the fast camera BD is static and closely represents the background light. Usually, the next two modes approximate a quadrature pair, and if they are recombined, the dominant rotating mode can be seen. By comparing the light oscillations to measurements of the edge magnetic field [17], we observe a *decrease* in local light emission corresponding to a *decrease* in the local poloidal magnetic field. Additionally, the frequency spectrum of the light oscillations correspond to the frequency spectrum of the magnetic oscillations measured by the shell-mounted Mirnov coils [29]. In the attached supplementary materials (stacks.iop.org/PPCF/57/045008)[1], we include videos that show the original camera data from Shot 77324 and a reconstruction of the temporal and spatial behavior of the light emission caused by the rotating $m/n = 3/1$ kink mode.

In addition to extracting the structure of plasma light fluctuations, the BD method can be used to measure a plasma's

[1] Supplementary Materials: three videos are attached in MPEG-4 format and require an MP4 viewer. The files are: (*i*) SUPPLEMENTARY-VIDEO-77324-FULL.MP4, (*ii*) SUPPLEMENTARY-VIDEO-77324-BD.MP4, and (*iii*) SUPPLEMENTARY-VIDEO-78029-BD.MP4. These files show high-speed video records corresponding to figures 6 and 7 in the body of the main text.

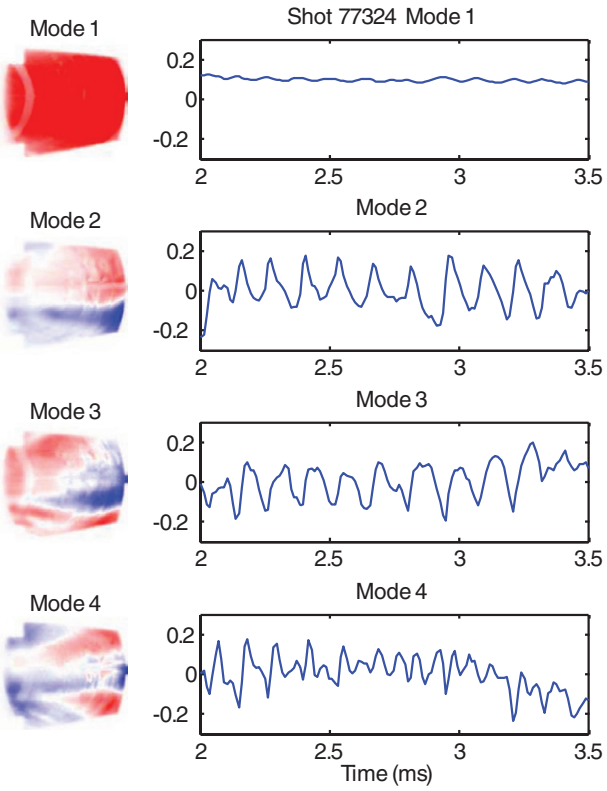


Figure 6. The first four modes from a biorthogonal decomposition of the fast camera data for unforced Shot 77324. The spatial modes are on the left and follow the same color bar as in figure 5. The temporal modes are on the right. Mode 1 is the equilibrium emission, while modes 2 and 3 form a quadrature pair representing a toroidally rotating mode at a frequency near 7 kHz. See also the supplementary materials (stacks.iop.org/PPCF/57/045008) for the full video records of this discharge.

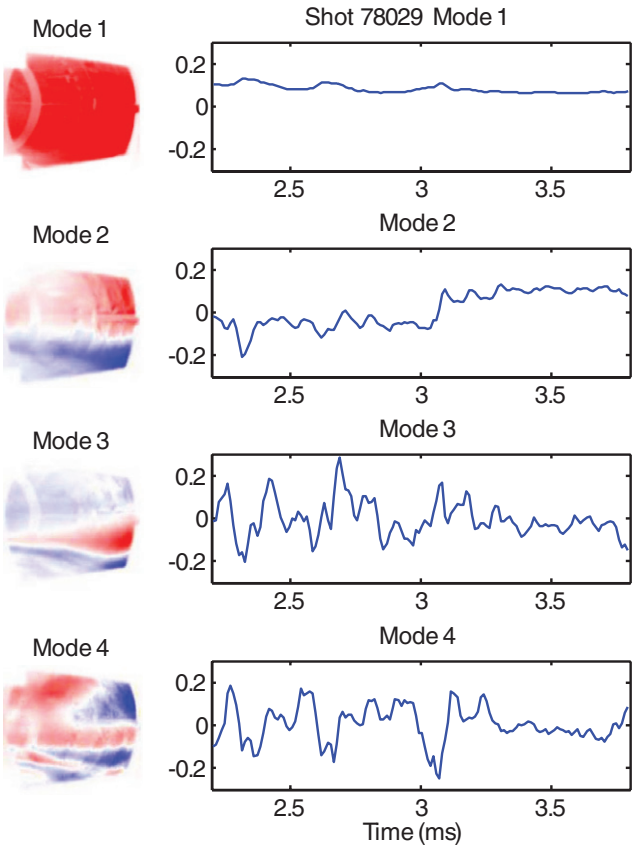


Figure 7. The BD modes for Shot 78029 with an RMP active from 2 to 4 ms. The effect of the phase flip can be seen in Mode 2 where the temporal mode resembles a step function. See also the video record of the resonant light emission available online in supplementary materials (stacks.iop.org/PPCF/57/045008).

static response to applied helical magnetic perturbations. These non-rotating, quasi-static perturbations resonate with the equilibrium magnetic field at the plasma's edge and are therefore known as resonant magnetic perturbations (RMPs). One particular RMP commonly used on HBT–EP is the phase flip [16–19]. A static $m/n = 3/1$ perturbation is introduced to a naturally rotating plasma, driving a static resonant mode that may influence the amplitude and rotation of the natural mode. After the plasma response settles, the polarity of the RMP is quickly reversed at 3.0 ms. After keeping the RMP held fixed in the reversed state for a certain amount of time, the RMP is turned off and the plasma returns to its unforced state. The result of performing a BD on fast camera data from Shot 78029, a phase flip shot, is shown in figure 7. The spatial modes are quite similar to those in Shot 77324, as shown in figure 6, however the second temporal mode displays a step-like function which is the result of the mode's resonance with the phase flip. This observation is similar to previous measurements which compared the magnetic structure of the helical plasma response resulting from quasi-static RMPs with the helical structure of naturally occurring edge kink modes [17]. Supplementary materials (stacks.iop.org/PPCF/57/045008) (online) show the temporal and spatial reconstruction of the light emission before, during, and after the application of the RMP.

5. Plasma response to RMPs under different conditions

The phase and amplitude of the RMP can be changed as well as characteristics of the plasma itself. In the case where the toroidal phase of the RMP is changed while the plasma settings are held constant, the overall fast camera BD doesn't change much. The temporal behavior is the same in each case and the phase flip is always at Mode 2. What does change is the spatial part. Figure 8 shows eight different shots, each taken with an RMP applied with a different toroidal phase. From the fast camera data it is apparent which of the programmed phases were used for the RMP.

If the toroidal phase of the RMP is held constant while the safety factor of the plasma or amplitude of the RMP is changed, different effects are apparent. In order to make comparisons, a quantitative measurement of the intensity of the plasma's response is required. This is achieved by extracting the fast camera mode that displayed the strongest step reaction to the phase flip, which is typically Mode 2. The root mean square of the spatial mode is multiplied by the singular value and the temporal mode. This produces a step-like signal which describes the overall light response to the phase flip. The measured static modulation in the light emission due to the RMP shows the same phase relationship

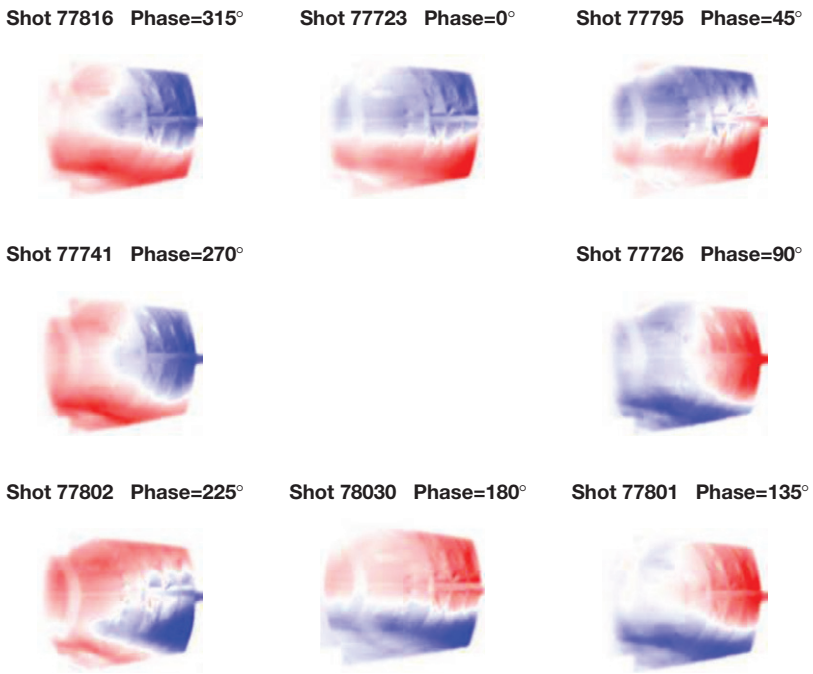


Figure 8. Spatial modes from phase-flip shots having RMPs applied with different toroidal angles. The $n = 1$ nature of the plasma response can be seen by comparing positive and negative perturbed emission regions with the applied phases. The color bar is the same as in figure 5(*a*).

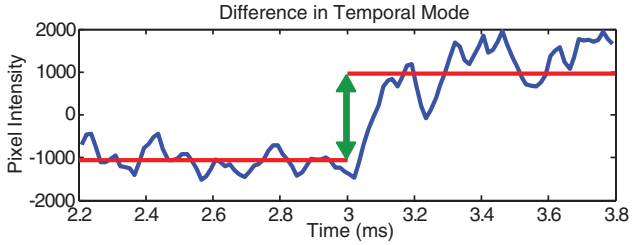


Figure 9. An example calculation of the plasma's response to the RMP, as quantified by the difference in the average light signal before and after the phase flip. The signal is taken from the BD mode that most closely resembles the applied perturbation.

between the visible light pattern and the perturbed poloidal magnetic field seen in naturally rotating kink modes, like that in figure 6. Taking the averages of this signal before and after the phase flip and then subtracting them produces a numerical quantity that can be compared under different plasma conditions. An example of this calculation can be seen in figure 9.

In the case where the RMP is held constant at $B_r^{3/1}/B_T = 0.001$ but the safety factor of the plasma is changed, a stronger response to the RMP can be seen when the safety factor at the edge, q_a is closer to 3. This result is shown in figure 10. The measured response with the camera is consistent with previous results using the magnetic signals [16, 17]. The calculation done using the magnetic signals is in black, while the fast camera response is in red. There is no absolute relationship between the fast camera's pixel intensity and the magnetic field strength, so this plot shows the relative trends because the light intensity scale is arbitrary. This variation in the plasma's RMP response with edge q is important, and we measure this variation independently using either

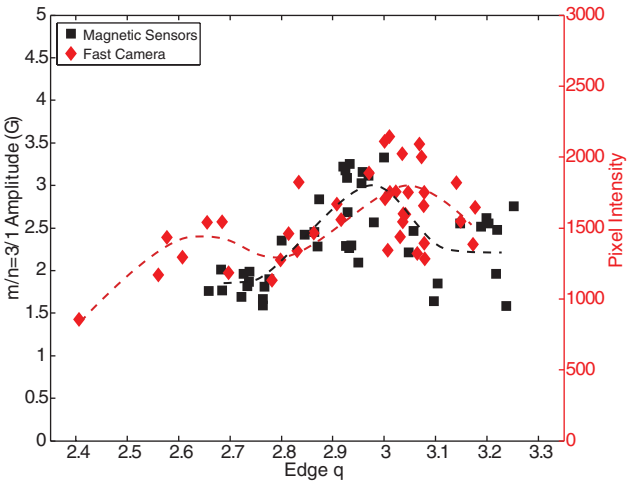


Figure 10. The magnetic data (black) and fast camera data (red) showing the plasma's response to the RMP for shots with different q_a (edge safety factor) values.

magnetic or light fluctuations. Nevertheless, the explanation for this variation is still under investigation.

If the RMP amplitude is increased, linear theory predicts that the plasma's response will increase as well. To test this hypothesis, the RMP amplitude was doubled and the plasma response was measured under different safety factors. The two datasets can be classified by the ratio of the imposed resonant radial magnetic field strength to the toroidal field, $B_r^{3/1}/B_T$: 0.001 and 0.002. Figure 11(*a*) shows a comparison of the plasma response at these two different amplitudes as measured by the magnetic data [30]. Figure 11(*b*) shows the same results with the fast camera data. Both measurement methods indicate that there is a

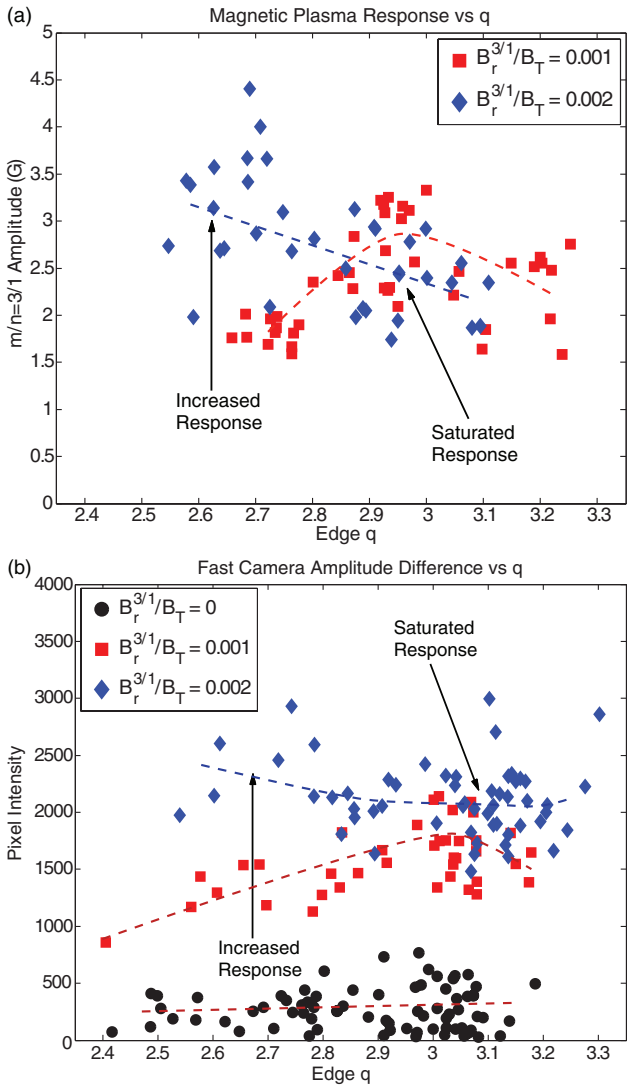


Figure 11. The plasma response versus q_a at two RMP amplitudes (red and blue) as measured by the magnetic sensors (*a*) and the fast camera (*b*). The first plot is adapted from [30] and the second plot includes the response from unforced plasmas (black).

saturation of the plasma's response to the RMP at higher safety factors.

6. Summary and future work

This work represents the first experiments performed using a high-speed camera on HBT–EP and the first video observations of long wavelength kink modes in a wall-stabilized tokamak. The dominant wavelength of visible light was determined to be 656 nm or Dα light and is consistent with the expected light emitted from a predominantly deuterium-fuelled plasma. A hollow profile is observed when an Abel inversion is used on the light recorded from the midplane. The fast camera can successfully determine the response of the plasma to a resonant magnetic perturbation. The toroidal angle of the RMP can be determined from the fast camera BD spatial mode shape. The RMP response amplitudes calculated from the fast camera are consistent with similar measurements made from the magnetic sensors.

On the HBT–EP tokamak, opportunities exist for future studies using more than one camera. Multiple cameras angles could allow for more complete inversions, perhaps creating full 3D profiles. In addition, as fast camera technology improves, camera data could be used to provide measurements for feedback as well.

Acknowledgments

The author would like to express appreciation for the help received from Dr Stephen Paul. He is greatly missed. She would also like to thank her colleagues on HBT–EP, and especially Jim Andrello and Nick Rivera. No project is ever an independent endeavor. This work has been supported by the US Department of Energy Grant DE-FG02-86ER53222 and the PPPL Off-Site University Research Program.

References

[1] Severo J H F *et al* 2007 Plasma rotation measurement in small tokamaks using an optical spectrometer and a single photomultiplier as detector *Rev. Sci. Instrum.* **78** 043509
[2] Zweben S, McChesney J and Gould R 1983 Optical imaging of edge turbulence in the Caltech tokamak *Nucl. Fusion* **23** 825
[3] Stratton B C *et al* 2004 Initial operation of the national spherical torus experiment fast tangential soft x-ray camera *Rev. Sci. Instrum.* **75** 3959–61
[4] Yu J H *et al* 2008 Fast imaging of edge localized mode structure and dynamics in DIII-D *Phys. Plasmas* **15** 032504
[5] Antar G *et al* 2009 On the onset of type I edge localized modes *Nucl. Fusion* **49** 032001
[6] Kirk A *et al* 2005 Structure of ELMs in MAST and the implications for energy deposition *Plasma Phys. Control. Fusion* **47** 315
[7] Ghendrih P *et al* 2003 Patterns of ELM impacts on the JET wall components *J. Nuclear Mater.* **313–6** 914–8
[8] Yu J H and Zeeland M A V 2008 Spectrally filtered fast imaging of internal magnetohydrodynamic activity in the DIII-D tokamak *Rev. Sci. Instrum.* **79** 10F516
[9] Yu J *et al* 2009 Fast camera imaging of dust in the DIII-D Tokamak *J. Nuclear Mater.* **390–1** 216–9 (*Proc. of the 18th Int. Conf. on Plasma-Surface Interactions in Controlled Fusion Device*)
[10] Kirk A *et al* 2012 Observation of lobes near the X point in resonant magnetic perturbation experiments on MAST *Phys. Rev. Lett.* **108** 255003
[11] Zweben S *et al* 2004 High-speed imaging of edge turbulence in NSTX *Nucl. Fusion* **44** 134
[12] Vianello N *et al* 2013 3D effects on the RFX-mod boundary *Nucl. Fusion* **53** 073025
[13] Haskey S R *et al* 2014 Synchronous imaging of coherent plasma fluctuations *Rev. Sci. Instrum.* **85** 033505
[14] Haskey S *et al* 2014 Visible light tomography of MHD eigenmodes in the H-1NF stellarator using magnetic coordinates *Nucl. Fusion* **54** 083031
[15] Maurer D A *et al* 2011 The high beta tokamak-extended pulse magnetohydrodynamic mode control research program *Plasma Phys. Control. Fusion* **53** 074016
[16] Maurer D A *et al* 2012 High resolution detection and excitation of resonant magnetic perturbations in a wall-stabilized tokamak *Phys. Plasmas* **19** 056123

[17] Shiraki D *et al* 2013 Measurement of 3D plasma response to external magnetic perturbations in the presence of a rotating external kink *Phys. Plasmas* **20** 102503
[18] Shilov M *et al* 2004 Dynamical plasma response of resistive wall modes to changing external magnetic perturbations *Phys. Plasmas* **11** 2573–9
[19] Mauel M *et al* 2005 Dynamics and control of resistive wall modes with magnetic feedback control coils: experiment and theory *Nucl. Fusion* **45** 285
[20] Rath N *et al* 2013 Adaptive control of rotating magnetic perturbations in HBT–EP using GPU processing *Plasma Phys. Control. Fusion* **55** 084003
[21] Rath N *et al* 2012 High-speed, multi-input, multi-output control using GPU processing in the HBT-EP tokamak *Fusion Eng. Des.* **87** 1895–9
[22] Vision research 2014 Phantom camera products: high speed cameras
[23] SCHOTT North America Inc 2014 *Wound Fiber Optic Image Bundles* (www.us.schott.com/lightingimaging/english/products/machinevision/fiberoptics/wound.html)
[24] Álvarez R, Rodero A and Quintero M 2002 An Abel inversion method for radially resolved measurements in the axial injection torch *Spectrochim. Acta B: At. Spectrosc.* **57** 1665–80
[25] Stotler D P *et al* 1996 Modeling of neutral hydrogen velocities in the tokamak fusion test reactor *Phys. Plasmas* **3** 4084–94
[26] Dudok de Wit T *et al* 1994 The biorthogonal decomposition as a tool for investigating fluctuations in plasmas *Phys. Plasmas* **1** 3288–300
[27] Grierson B A, Worstell M W and Mauel M E 2009 Global and local characterization of turbulent and chaotic structures in a dipole-confined plasma *Phys. Plasmas* **16** 055902
[28] Levesque J *et al* 2013 Multimode observations and 3D magnetic control of the boundary of a tokamak plasma *Nucl. Fusion* **53** 073037
[29] Angelini S 2014 High speed videography on HBT-EP *PhD Thesis* Columbia University, New York
[30] Shiraki D 2012 High-resolution MHD spectroscopy of external kinks in a tokamak plasma *PhD Thesis* Columbia University, New York